Numerical analysis of a 2-D viscous sintering problem with non smooth boundaries

EINDHOVEN UNIVERSITY OF TECHNOLOGY
Department of Mathematics and Computing Science

RANA 92-01
January 1992

NUMERICAL ANALYSIS OF A 2-D VISCOUS SINTERING PROBLEM WITH NON SMOOTH BOUNDARIES

by
G.A.L. van de Vorst
R.M.M. Mattheij

ISSN: 0926-4507
Reports on Applied and Numerical Analysis
Department of Mathematics and Computing Science
Eindhoven University of Technology
P.O. Box 513
5600 MB Eindhoven
The Netherlands

Numerical Analysis of a 2-D Viscous Sintering Problem with Non Smooth Boundaries

G.A.L. van de Vorst
R.M.M. Mattheij

Abstract

By viscous sintering it is meant the process of bringing a granular compact to a temperature at which the viscosity of the material becomes low enough for surface tension to cause the particles to deform and coalesce, whereby the material transport can be modelled as a viscous incompressible newtonian volume flow. Here a two-dimensional model is considered. A Boundary Element Method is applied to solve the governing Stokes creeping flow equations for an arbitrarily initial shaped fluid region. In this paper we show that the viscous sintering problem is well-conditioned from an evolutionary point of view. However as boundary value problem at each time step, the problem is ill-conditioned when the contact surfaces of the particles are small, i.e. in the early stages of the coalescence. This is because the curvature of the boundary at those places can be very large. This ill-conditioning is illustrated by an example: the coalescence of two equal circles. This example demonstrates the main evolutionary features of the sintering phenomenon very well. A numerical consequence of this ill-conditioning is that special care has to be taken for distributing and redistributing the nodal points at those boundary parts. Therefore an algorithm for this node redistribution is outlined. Several numerical examples sustain the analysis.

A.M.S. Classifications: 65R99, 76D07
Keywords : sintering, viscosity, boundary element method, moving boundaries.

1 Introduction

Sintering is the process of bringing a powder of metals, ionic crystals, or glasses (a compact) to such a high temperature that sufficient mobility is present to release the excess free energy of the surface of the powder, thereby joining the particles together. The driving force arises from the excess free energy of the surface of the powder over that of the solid material. For a survey of the most important papers about sintering we refer to the book edited by Sōmiya and Moriyoshi [11].

We are interested in the case of sintering glasses, see also [7] or [13]. There, the material transport can be modelled as a viscous incompressible Newtonian volume flow, driven solely by surface tension (viscous sintering), i.e. the Stokes creeping flow equations hold. The geometry of such a sintering compact is mostly very complex. Because of this it is impossible to give a deterministic description of the flow in such a compact as a whole. We shall therefore investigate simple geometries; to start with in 2-D only, aiming at eventually deriving constitutive laws of the effects obtained.

Analytical solutions for certain classes of two-dimensional viscous sintering problems are recently be obtained by Hopper [3] and [4]. Among these is the coalescence of two equal circles, which is a classical problem in sintering literature. A numerical simulation of the sintering of an infinite line of circles was performed by Ross *et al* [10]. They were the first who applied a Finite Element Method to the problem. However, they obtained a growth of the contact line between those circles which was differing from experimental results in known literature. Jagota and Dawson [6] have reported about the evolution of two spheres and an infinite line of spheres (three-dimensional axisymmetric problems), using a Finite Element Method. Recently, Kuiken [7] applied a Boundary Element Method to solve viscous sintering problems for bodies with rather smooth boundaries. In previous work of us, i.e. [12] and [13], we used a Boundary Element Method to solve the problem for an arbitrarily shaped fluid region. In those papers, we also discussed the numerical problems that can arise in computing the curvature of the shape, in particular at places where a cusp is arising.

In this paper we investigate whether the viscous sintering problem as described in detail in the next section, is well-conditioned from an *evolutionary* point of view and as *boundary value* problem at each time step as well. We then consider the numerical consequences of the conditioning of these problems. It turns out that special care has to be taken when the nodal points are redistributed. Therefore a special algorithm for the node redistribution has been developed, which is suitable for problems where the curvature of the boundary is the driving force. Such a kind of precise grid generation technique is also performed, for example, by Dritschel [1]. The methods he developed are an extension on the technique called "contour dynamics", which is used in two dimensional vortex dynamics. However, the properties he uses to redistribute the nodes differ completely from ours; this is because the type of problem is quite different from ours.

This paper is built up as follows: In the next section we first formulate the problem; after which we shall go deeper into the question of the conditioning

of the sintering problem on the basis of a simple but typical example, viz. the evolution of the coalescence of two equal circles. This example demonstrates the main features of the simulation of the sintering phenomenon very well as will be shown in section 3. More than that, for this example the coalescence can be solved analytically, as has recently been shown by Hopper [3]. By using this analytical solution we are able to give a fairly quantitative sensitivity analysis; i.e. we can investigate the influence of a perturbation of the initial radius R, the contact radius r and the neck curvature on the shape and curvature of the region where those circles are touching. Then, in section 5 we briefly discuss the Boundary Element Method, which is used to solve the problem numerically. Furthermore we give an algorithm for distributing the nodal boundary points and discuss the numerical implementation of it. Finally, in section 6 we show some numerical results for simply connected surfaces.

2 Problem Formulation

We model the viscous sintering problem by the Stokes creeping flow equations, i.e. the flow is a viscous incompressible Newtonian fluid, see also Kuiken [7]. The *two dimensional* fluid region is assumed to be *simply connected* and is defined by a closed curve Γ with interior domain Ω. We denote the dimensionless velocity field of the fluid by $\mathbf{v}$ and the dimensionless pressure by p.

The Stokes creeping flow equations in dimensionless form read,

$$\begin{aligned} \triangle \mathbf{v} - \operatorname{grad} p &= 0 \\ \operatorname{div} \mathbf{v} &= 0, \end{aligned} \tag{1}$$

with stress tensor $\mathcal{T}$, given by

$$\mathcal{T}_{ij} = -\delta_{ij} p + \left(\frac{\partial v_i}{\partial x_j} + \frac{\partial v_j}{\partial x_i} \right). \tag{2}$$

The driving force of the boundary movement is a tension in the normal direction on the boundary, which is proportional to the local curvature (κ) of the boundary. This boundary condition can be described as

$$\mathcal{T}\mathbf{n} = (\operatorname{div} \mathbf{n})\,\mathbf{n} = \kappa \mathbf{n}, \tag{3}$$

where $\mathbf{n}$ is the outward unit normal vector of the boundary.

In principle, the above equations can be solved for a *fixed* boundary Γ, which gives the velocity field $\mathbf{v}$ of this boundary. The displacement of the boundary can be obtained from this boundary velocity field, in the following way,

$$\frac{d\mathbf{x}}{dt} = \mathbf{v}(\mathbf{x}) \qquad (\mathbf{x} \in \Gamma), \tag{4}$$

where t is the dimensionless time. The above equation is expressing that that the *material* points of the boundary are moving in the direction of the *characteristic* curves.

Our only interest is the movement of the boundary Γ. Hence only the velocity at the boundary is required, from which we can calculate the shape evolution of the body directly. Therefore this problem is ideally suited to be solved numerically by a Boundary Element Method (BEM). To do this, we have to reformulate the problem as an integral equation over the boundary. This is done in terms of boundary distributions of hydrodynamical single- and double-layer potentials, see also Ladyzhenskaya [8].

When the boundary is sufficiently "smooth", the integral formulation that can be derived for the Stokes equations at a point, say $\mathbf{x}$, reads in matrix notation (see also [13])

$$\mathcal{C}\,\mathbf{v}(\mathbf{x}) + \int_\Gamma \mathcal{Q}(\mathbf{x},\mathbf{y})\,\mathbf{v}\,d\Gamma_y = \int_\Gamma \mathcal{U}(\mathbf{x},\mathbf{y})\,\mathbf{b}\,d\Gamma_y. \tag{5}$$

Here $\mathcal{C}$,$\mathcal{Q}(\mathbf{x},\mathbf{y})$ and $\mathcal{U}(\mathbf{x},\mathbf{y})$ are 2×2 matrices with coefficients c_{ij}, q_{ij} and u_{ij} respectively:

$$c_{ij} = \begin{cases} \delta_{ij} & \mathbf{x} \in \Omega \\ \frac{1}{2}\delta_{ij} & \mathbf{x} \in \Gamma, \end{cases} \tag{6}$$

$$q_{ij} = \frac{r_i r_j}{\pi(r_1^2 + r_2^2)^2} r_k n_k, \tag{7}$$

$$u_{ij} = \frac{1}{4\pi}\Big[-\delta_{ij}\frac{1}{2}\log[r_1^2 + r_2^2] + \frac{r_i r_j}{r_1^2 + r_2^2}\Big], \tag{8}$$

where δ_{ij} is the Kronecker delta, $r_i = x_i - y_i$, and the vector $\mathbf{b}$ is the boundary curvature in the normal direction, i.e.

$$\mathbf{b} = \kappa\,\mathbf{n}. \tag{9}$$

The integral equation (5), or the equations (1)-(3), which have to be solved for a fixed boundary, do not ensure a unique solution $\mathbf{v}$. It can be seen, cf [13], that a superposition of an arbitrary rigid-body *translation* or *rotation* upon any particular solution of these equations, is also a solution of equations (1)-(2) and will not alter the stress field at the boundary. Hence, in total we need to add three extra conditions (equations) for obtaining the velocity field of a fixed boundary.

We follow the approach of Hsiao, Kopp and Wendland [5], for making the integral equation (5) uniquely solvable for a fixed boundary. This is done by adding three additional variables w_i to this integral equation which prescribe the translation and rotation, i.e.

$$\mathcal{C}\,\mathbf{v}(\mathbf{x}) + \int_\Gamma \mathcal{Q}(\mathbf{x},\mathbf{y})\,\mathbf{v}\,d\Gamma_y + \mathcal{V}(\mathbf{x})\,\mathbf{w} = \int_\Gamma \mathcal{U}(\mathbf{x},\mathbf{y})\,\mathbf{b}\,d\Gamma_y, \tag{10}$$

where $\mathcal{V}$ is a 2×3 matrix defined by

$$\mathcal{V} = \begin{bmatrix} 1 & 0 & x_2 \\ 0 & 1 & -x_1 \end{bmatrix}. \tag{11}$$

Now, three equations have to be given to ensure that the boundary velocity is defined uniquely. In order to prescribe the translation freedom, we formulate

the problem to be stationary at a (reference) point in the fluid, say $\mathbf{x}^r$. With regard to this reference point the velocity of the boundary points is computed. The most natural choice for this reference point is the centre of mass: the point where the gravity forces would grip the body, thus:

$$\mathbf{v}(\mathbf{x}^r) = 0. \tag{12}$$

Using this, we derive from the integral formulation (5) and $\mathbf{x} = \mathbf{x}^r$ the following two equations

$$\int_\Gamma \mathcal{Q}(\mathbf{x}^r, \mathbf{y})\, \mathbf{v}\, d\Gamma_y = \int_\Gamma \mathcal{U}(\mathbf{x}^r, \mathbf{y})\, \mathbf{b}\, d\Gamma_y. \tag{13}$$

Furthermore we assume the tangential component of the velocity at the boundary is zero (one equation), i.e.

$$\int_\Gamma (\mathbf{v}, \tau)\, d\Gamma \;=\; 0, \tag{14}$$

where τ is the tangential vector of the boundary. Combining this with Stokes formula it follows from equation (14) that the flow in Ω is *irrotational.*

3 The Analytical Solution for the coalescence of two equal circles

In this section we give the analytical solution for the coalescence of two equal circles and we introduce some notation for the main properties of this evolution. These are the initial radius R of both circles, the measure of contact between both circles and the boundary curvature at the contact.

The coalescence of two equal circles demonstrates the main features of the simulation of the sintering phenomenon very well. In the early stage of the coalescence, the curvature of the boundary is very large in the region where both circles are touching (almost a *cusp*); at later stages the shape is becoming "smoother", i.e. the curvature is varying only moderately everywhere.

The analytical solution for the evolution of two equal coalescing circles has recently been derived by Hopper [3], subsection **4.4**. He described the evolution of these circles in terms of a time-dependent mapping function $z = x + iy = \Omega(\xi, t)$ of the unit circle, conformal on $|\xi| \leq 1$. The time evolution of the map was given in parametric form. In these papers, the equations derived are valid for the coalescence of two circles with initial radius $\frac{1}{2}\sqrt{2}$.

Following Hopper [3], we can derive parametric equations for the evolution of two coalescing circles both with initial radius R and centres $(R, 0)$ and $(-R, 0)$ each

$$\begin{aligned} x(\theta, \nu) &= \frac{(1-\nu^2)(1-\nu)R\sqrt{2}\cos\theta}{(1 - 2\nu\cos 2\theta + \nu^2)\sqrt{1+\nu^2}} \\ y(\theta, \nu) &= \frac{(1-\nu^2)(1+\nu)R\sqrt{2}\sin\theta}{(1 - 2\nu\cos 2\theta + \nu^2)\sqrt{1+\nu^2}} \end{aligned} \tag{15}$$

and for the time t (as function of ν)

$$t(\nu) = \frac{\pi R}{\sqrt{2}} \int_{\nu}^{1} \frac{dk}{k\sqrt{1+k^2}\mathrm{K}(k)}. \tag{16}$$

Here $\mathrm{K}(k)$ is the complete elliptic integral of the first kind defined by

$$\mathrm{K}(k) = \int_{0}^{\frac{\pi}{2}} \left(1 - k^2 \sin^2\varphi\right)^{-\frac{1}{2}} d\varphi. \tag{17}$$

The degree of coalescence is specified by the parameter ν, which decreases from 1 to 0 if time increases (t is going to infinity as $\nu \to 0$), and the boundary curve is specified by the parameter θ which is varying from 0 to 2π. Remark that at $t = 0$, both circles are making contact in the origin.

Of special interest is the region where the circles are touching. In sintering literature, see for example Sōmiya and Moriyoshi [11], this contact region is usually called the *neck region*. In our example, the line of contact is the Y-axis during the evolution. Let r be the *contact radius* between both circles, and denote the point on the boundary at the line of contact in the positive direction by $\mathbf{x}^n$, i.e. $\mathbf{x}^n = (0, r)$. In the remainder of this paper we call this point the *neck*.

The development during sintering of the contact radius is also of physical interest. This contact radius is a measure of how "strong" a sintering compact already is. When this contact radius is small, a smaller force is necessary to brake the contact between both circles than at later stages of the sintering process, when the contact radius is larger.

In the analytical solution (15) the neck is occurring at $\theta = \pi/2$ during the evolution. Thus for the contact radius r, as function of the parameter ν, the following holds

$$r(\nu) = y(\frac{\pi}{2}, \nu) = \frac{(1-\nu)R\sqrt{2}}{\sqrt{1+\nu^2}}. \tag{18}$$

Note that as $\nu \to 0$, i.e. $t \to \infty$, then $r \to R\sqrt{2}$; which is the radius of the circle that the shape evolution approaches as the time increases.

We obtain by elimination for the parameter ν as function of the contact radius r, from (18)

$$\nu = \nu(r) = \frac{2R^2 - r\sqrt{4R^2 - r^2}}{2R^2 - r^2}. \tag{19}$$

For the curvature of the neck, say κ_n, we can derive from the parametric equations (15)

$$\begin{aligned} \kappa_n(\nu) &= \left. \frac{x_{\theta\theta} y_\theta - x_\theta y_{\theta\theta}}{(x_\theta^2 + y_\theta^2)^{\frac{3}{2}}} \right|_{\theta=\frac{\pi}{2}} \\ &= -\frac{(1 - 6\nu + \nu^2)\sqrt{1+\nu^2}}{(1-\nu)^3 R\sqrt{2}}. \end{aligned} \tag{20}$$

Remark that as $\nu \to 0$, i.e. $t \to \infty$, then $\kappa_n \to -1/R\sqrt{2}$, as assumed. The derived neck curvature (20) can be written as a function of the contact radius r; from equations (19) and (20), we obtain

$$\kappa_n(r) = \frac{4R^2}{r^3} - \frac{3}{r}. \tag{21}$$

This is an interesting result on it's own, which also can be used for the perturbation analysis which is performed out in the next sections.

Not only the curvature κ of the neck point can be written as a function of the contact radius r, i.e. equation (21). The shrinkage of the two circles can also be described as a function of the contact radius. Let therefore s be defined as the *shrinkage* of both circles, i.e.

$$s = 2R - x(0, \nu). \tag{22}$$

From equations (15) and (18) follows

$$\begin{aligned} s &= 2R - \frac{(1+\nu)R\sqrt{2}}{\sqrt{1+\nu^2}} \\ &= 2R - \frac{(1+\nu)r}{1-\nu}. \end{aligned} \tag{23}$$

With equation (19) we eliminate ν from (23), we obtain

$$s = 2R - \sqrt{4R^2 - r^2}. \tag{24}$$

4 Perturbation Analysis of the Analytical Solution

In this section we shall investigate the influence of a perturbation of the initial radius R, the contact radius r and the neck curvature on the shape and curvature of the neck. From this analysis we shall draw conclusions about the conditioning of the above described problem as an evolutionary problem and as boundary value problem at each time step as well.

4.1 Perturbation of the initial radius R

In the following analysis, we show that a small perturbation of the initial radius R of both circles, will not perturb the evolution of the shape of the neck region significantly, while the neck curvature is changing dramatically.

Here we are interested in the change of the shape of two coalescing equal circles both with initial radius R each and with $R + \varepsilon$ ($\varepsilon \ll 1$) each, considered for the *same* contact radius r (figure 1); note that the shapes are taken at a *different* time t and $\tilde{t}$, say, respectively. Thus we have to consider the parametric equations

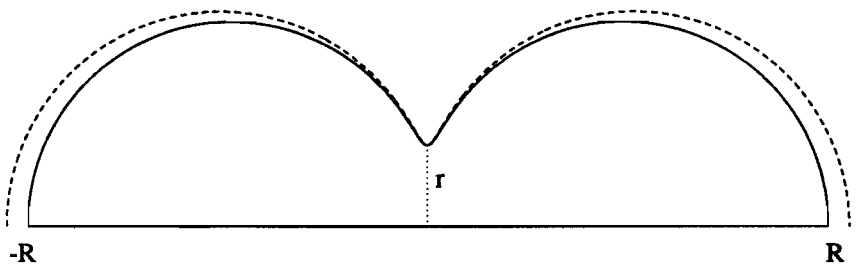

Figure 1: The coalescence of two equal circles with both initial radii R and $R+\varepsilon$ respectively.

(15) as function of R and t (i.e. ν). A measure for the difference between both shapes is given by the derivative of x, y with respect to R.

Using (18), the parametric equations (15) can be written as

$$\begin{aligned} x(\theta,\nu) &= \frac{r(1-\nu^2)\cos\theta}{1+\nu^2-2\nu\cos 2\theta} \\ y(\theta,\nu) &= \frac{r(1+\nu)^2\sin\theta}{1+\nu^2-2\nu\cos 2\theta}. \end{aligned} \tag{25}$$

For the derivative of ν with respect to R, we obtain after squaring, taking the derivative from equation (18) and using the relation (19)

$$\frac{\partial\nu}{\partial R} = \frac{2R(1-\nu)^2}{r\sqrt{4R^2-r^2}}. \tag{26}$$

By taking the derivative of the parametric equations (25) with respect to R and using (26), we derive

$$\begin{aligned} \frac{\partial x}{\partial R} &= \frac{4R(1-\nu)^2[(1+\nu^2)\cos 2\theta - 2\nu]\cos\theta}{\sqrt{4R^2-r^2}(1+\nu^2-2\nu\cos 2\theta)^2} \\ \frac{\partial y}{\partial R} &= \frac{8R(1+\nu)(1-\nu)^3\sin\theta\cos^2\theta}{\sqrt{4R^2-r^2}(1+\nu^2-2\nu\cos 2\theta)^2}. \end{aligned} \tag{27}$$

We can find upper bounds for those derivatives as follows. Because of symmetry, we only look at the first quadrant of the shape, i.e. $\theta \in [0,\pi/2]$ and $x,y \geq 0$. After substituting $\xi = \cos\theta$ and $\tilde{r} = r/(\sqrt{2}\,R)$ in (27) we derive

$$\begin{aligned} \frac{\partial x}{\partial R} &= \frac{2\sqrt{2}(1-\nu)^2[2(1+\nu^2)\xi^2-(1+\nu)^2]\xi}{\sqrt{2-\tilde{r}^2}((1+\nu)^2-4\nu\xi^2)^2} \\ \frac{\partial y}{\partial R} &= \frac{4\sqrt{2}(1+\nu)(1-\nu)^3\xi^2\sqrt{1-\xi^2}}{\sqrt{2-\tilde{r}^2}((1+\nu)^2-4\nu\xi^2)^2}. \end{aligned} \tag{28}$$

Note that the parameters ξ, ν and $\tilde{r}$ are varying between 0 and 1. Furthermore, we are mainly interested in the change of the shape of the neck region, i.e. ξ is small. Using (25) and

$$\frac{1-\nu}{1+\nu} = \frac{\tilde{r}}{\sqrt{2-\tilde{r}^2}}, \tag{29}$$

we derive from (28)

$$\begin{aligned} \frac{\partial x}{\partial R} &= \frac{2xy[2(1+\nu^2)\xi^2 - (1+\nu)^2]}{Rr(2-\tilde{r}^2)(1+\nu)^2\sqrt{1-\xi^2}} \\ \frac{\partial y}{\partial R} &= \frac{2\sqrt{2}\,xy\xi}{R^2(2-\tilde{r}^2)^{\frac{3}{2}}}. \end{aligned} \tag{30}$$

When $\xi = 0$, the expression $|2(1+\nu^2)\xi^2 - (1+\nu)^2|$ is maximal $(= (1+\nu)^2)$ as a function of ξ. From this and $0 \leq \tilde{r} < 1$, the following upper bounds are obtained

$$\left|\frac{\partial x}{\partial R}\right| \leq \frac{2xy}{Rr\sqrt{1-\xi^2}} \qquad \text{and} \qquad \left|\frac{\partial y}{\partial R}\right| \leq \frac{2\sqrt{2}\,xy}{R^2}. \tag{31}$$

Remark that in the neck region (y/r) is bounded and x is small. From this and the estimates (31) we conclude that a perturbation of the initial radius R of the coalescing circles will not change much the shape of the neck region measured at a point where the contact radius r is the same for both, even when r is small, as can also be observed in figure 1.

However, the *neck curvature* does change dramatically when the contact radius is small. This can be illustrated by computing the derivative of the curvature with respect to R in the neck. From the relation for the exact neck curvature (21), this derivative by constant radius r is given by

$$\frac{\partial \kappa_n}{\partial R} = \frac{8R}{r^3}. \tag{32}$$

This derivative becomes very large when the contact radius r is small, i.e. the curvature may change a lot from a very small perturbation of the initial radius of the two coalescing circles!

A measure for the difference between t and $\tilde{t}$ is given by the derivative of t with respect to R, i.e. taking the derivative of equation (16) and using (18) and (26), we find

$$\frac{\partial t}{\partial R} = \frac{t}{R} - \frac{\pi\tilde{r}\sqrt{1+\nu^2}}{\nu \mathrm{K}(\nu)\sqrt{2(2-\tilde{r}^2)}}. \tag{33}$$

From the asymptotic expansions for the complete elliptic integral $\mathrm{K}(\nu)$, i.e. equations 8.113.1 and 8.113.3 of Gradshteyn and Ryzhik [2],

$$\begin{aligned} \mathrm{K}(\nu) &= \frac{1}{2}\log\frac{16}{1-\nu^2} + \mathcal{O}\big((1-\nu^2)\log(1-\nu^2)\big) \qquad (\nu \to 1) \\ \mathrm{K}(\nu) &= \frac{\pi}{2}\Big[1 + \frac{1}{4}\nu^2 + \mathcal{O}(\nu^4)\Big] \qquad\qquad\qquad\quad (\nu < 1), \end{aligned} \tag{34}$$

we obtain that when the time t is not too large, say for values of $\nu > 0.1$, the derivative (33) is small. We conclude that when the initial radius R is perturbed, the time-scale of the neck evolution will not change much.

We conclude that the *global* shape of the neck region, by a given contact radius, is effectively independent of the initial radius R of both coalescing circles; although the curvature of the neck (*local* effect) can be rather different at an early stage of the coalescence.

4.2 The Evolution of the Neck Region

In the following analysis, we show that when the contact radius r is getting somewhat larger, the shape of the neck region is not perturbed significantly. However again, a small perturbation of the contact radius is changing the neck curvature dramatically! Furthermore we show that the neck evolution is a "smooth" function of the time.

For this we consider the shape of two coalescing equal circles both with initial radius R at time t when the contact radius is r and at time $\hat{t}$ with contact radius is $r+\varepsilon$ ($\varepsilon \ll 1$). Thus now, we have to consider the parametric equations (15) as function of r and t. The measure for the difference between both shapes is given by the derivative of x, y with respect to r.

For the derivative of ν with respect to r, we obtain after squaring, taking the derivative from equation (18) and using the relation (19)

$$\frac{\partial \nu}{\partial r} = -\frac{2R^2(1-\nu)^2}{r^2\sqrt{4R^2-r^2}}. \tag{35}$$

By taking the derivative of the parametric equations (25) with respect to r and considering only the first quadrant, we obtain after substitution of ξ, $\tilde{r}$ and (35)

$$\begin{aligned} \frac{\partial x}{\partial r} &= \frac{(1-\nu^2)\xi}{(1+\nu)^2-4\nu\xi^2} + \frac{2(1-\nu)^2[(1+\nu)^2-2(1+\nu^2)\xi^2]\xi}{\tilde{r}\sqrt{2-\tilde{r}^2}\,((1+\nu)^2-4\nu\xi^2)^2} \\ \frac{\partial y}{\partial r} &= \frac{(1+\nu)^2\sqrt{1-\xi^2}}{(1+\nu)^2-4\nu\xi^2} - \frac{4(1+\nu)(1-\nu)^3\xi^2\sqrt{1-\xi^2}}{\tilde{r}\sqrt{2-\tilde{r}^2}\,((1+\nu)^2-4\nu\xi^2)^2}. \end{aligned} \tag{36}$$

Again our interest is mainly the neck region, i.e. ξ is small. Using (25) and (29), we derive for (36)

$$\begin{aligned} \frac{\partial x}{\partial r} &= \frac{y\xi}{R\sqrt{2(1-\xi^2)(2-\tilde{r}^2)}} + \frac{y^2\xi\sqrt{2}[(1+\nu)^2-2(1+\nu^2)\xi^2]}{R(1-\xi^2)(1+\nu)^2(2-\tilde{r}^2)^{\frac{3}{2}}} \\ \frac{\partial y}{\partial r} &= \frac{y}{r} - \frac{2\sqrt{2}\,xy\xi}{r\,R(2-\tilde{r}^2)^{\frac{3}{2}}}. \end{aligned} \tag{37}$$

Following the procedure of subsection 4.1, we obtain as upper bounds

$$\left|\frac{\partial x}{\partial r}\right| \le \frac{y\xi}{R\sqrt{2(1-\xi^2)}}\left(1+\frac{2y}{\sqrt{1-\xi^2}}\right) \quad \text{and} \quad \left|\frac{\partial y}{\partial r}\right| \le \frac{y}{r}\left(1+\frac{2\sqrt{2}\,x\xi}{R}\right). \tag{38}$$

In the neck region y is $\mathcal{O}(r)$ and x small, i.e. from (38) we conclude again that a small change of the contact radius r of the coalescing circles will not perturb the shape of the neck region, even when r is small.

The relation (21) for the (exact) neck curvature gives also information about the effect of a change of the contact radius r on this curvature. From (21) it follows that the derivative of the neck curvature, with respect to r, is given by

$$\frac{\partial \kappa_n}{\partial r} = -\frac{12R^2}{r^4} + \frac{3}{r^2}. \tag{39}$$

Thus a small change of the contact radius r has an $\mathcal{O}\left(\frac{1}{r^4}\right)$ effect on the neck curvature, i.e. when the contact radius is small the curvature is changed dramatically. Conversely, we also have,

$$\frac{\partial r}{\partial \kappa_n} = -\frac{r^4}{12R^2 + 3r^2}, \tag{40}$$

i.e. a change of the neck curvature gives only an $\mathcal{O}(r^4)$ effect on the contact radius r.

A measure for the time difference between the shapes at time t and $\hat{t}$ is given by the derivative of t with respect to r, i.e. taking the derivative of equation (16) and using (18) and (35), we derive

$$\frac{\partial t}{\partial R} = \frac{\pi\sqrt{1+\nu^2}}{2\nu \mathrm{K}(\nu)\sqrt{2-\tilde{r}^2}}. \tag{41}$$

From the asymptotic expansions (34) follows that the derivative (41) is small, when the time t is not too large. We conclude that the neck evolution is a smooth function of the time.

The above analysis shows that a small change of the contact radius is hardly perturbing the global shape of the neck region. Only the curvature of the neck (a local effect) is changed dramatically when r is small.

4.3 Condition of Evolution and Boundary Value Problem

In the two previous subsections, we have shown that a perturbation of the initial radius R or the contact radius r is hardly changing the *global* shape of the neck region, even in the early stage of the coalescence, i.e. when the contact radius is small. However, the neck curvature is changed dramatically in both cases when r is small. This causes on the shape of the neck region an effect that is only very *locally* noticeable in the neighbourhood of the neck point.

From this, we conclude that the problem of two coalescing circles is well-conditioned from an evolutionary point of view. However, if we consider the problem that has to be solved for a fixed boundary at each time step, i.e. the boundary value problem, especially in the early stage of the coalescence; this problem is ill-conditioned because of the dramatically changing neck curvature.

In practice, this implies that we have to start with a shape that has a contact radius such that the neck curvature is not too large (we used order 10^3). Furthermore, we have shown that a change of the neck curvature does not result in a noticeable change of shape of the neck region. Therefore it is sufficient that the approximate neck curvature be of the *order* of the exact curvature, and that during the computation this approximate neck curvature is not changing significantly due to node redistribution.

5 Numerical Solution

In this section we shall assess the numerical consequences of the fact that the evolution problem is ill-conditioned as a boundary value problem at each time step when the neck curvature is large, i.e. the contact radius r is small. We first investigate the influence of a perturbation of the (boundary) discretization points on the approximate curvature, especially in the neck region. We then give an algorithm for distributing the nodal points. We also discuss the numerical implementation of the latter.

5.1 Numerical Discretization

The problem is ideally suited to be solved by a Boundary Element Method. Therefore the boundary will be discretized into a sequence of elements and the velocity and surface tension are written in terms of their values at a sequence of, say N, nodal points. From the discretized form of the integral equation (10) for every node, together with the discretized form of equations (13) and (14), we derive a system of (2N+3) linear algebraic equations with 2N+3 unknowns. More details of the implementation can be found in [12] and [13].

From this system we obtain the (approximate) velocity at time, say $t = t_k$, at the nodal boundary points. The displacement of the boundary at time $t_{k+1} = t_k + \Delta t$ can be obtained by discretizing equation (4). In early papers of us, we used a simple Forward Euler scheme. However sometimes, e.g. in the early stages of the coalescence of two equal circles, the system of ordinary differential equations that has to be solved for the displacement of the boundary is *stiff*. Because of this, it seems better to use a time integration method which is more suitable for stiff systems.

5.2 Perturbation Analysis of the Approximate Curvature

We consider the disturbance of the curvature when one of the discretization points of the boundary is moved slightly in one direction. Here, special interest is taken in the approximation of the curvature of the neck. Again we shall show that for a small perturbation of the boundary of the neck region the curvature is changed dramatically. This perturbation of the boundary is arising numerically from the

spatial discretization error, i.e. the error that is made by replacing the boundary through a polygon, and the *time* discretization error, i.e. the error that arises from a time stepping scheme.

An approximation for the curvature, say $\tilde{\kappa}$, of this discretized boundary is found by fitting a quadratic polynomial at the point $\mathbf{x}^2$, say, and its two neighbouring nodes, say $\mathbf{x}^1$ and $\mathbf{x}^3$ (see also [13]). The approximating curvature of the point $\mathbf{x}^2$ is computed as

$$\tilde{\kappa}(\mathbf{x}^2) \doteq \frac{4\left[(x_2^3 - x_2^1)(x_1^1 - 2x_1^2 + x_1^3) - (x_1^3 - x_1^1)(x_2^1 - 2x_2^2 + x_2^3)\right]}{((x_1^3 - x_1^1)^2 + (x_2^3 - x_2^1)^2)^{\frac{3}{2}}}. \tag{42}$$

We are interested in the change of the curvature when one of the coordinates of point $\mathbf{x}^k$ (k=1,2,3) is perturbed. A measure for the change of the approximate curvature of $\mathbf{x}^2$ by such a perturbation is given by the partial derivatives of $\tilde{\kappa}$ with respect to x_j^k, i.e.

$$\begin{aligned}
\frac{\partial\tilde{\kappa}}{\partial x_1^1} &= \frac{3(x_1^3-x_1^1)}{\ell^2}\tilde{\kappa} + \frac{8(x_2^3-x_2^2)}{\ell^3} & \frac{\partial\tilde{\kappa}}{\partial x_2^1} &= \frac{3(x_2^3-x_2^1)}{\ell^2}\tilde{\kappa} - \frac{8(x_1^3-x_1^2)}{\ell^3} \\
\frac{\partial\tilde{\kappa}}{\partial x_1^2} &= -\frac{8(x_2^3-x_2^1)}{\ell^3} & \frac{\partial\tilde{\kappa}}{\partial x_2^2} &= \frac{8(x_1^3-x_1^1)}{\ell^3} \\
\frac{\partial\tilde{\kappa}}{\partial x_1^3} &= -\frac{3(x_1^3-x_1^1)}{\ell^2}\tilde{\kappa} + \frac{8(x_2^2-x_2^1)}{\ell^3} & \frac{\partial\tilde{\kappa}}{\partial x_2^3} &= -\frac{3(x_2^3-x_2^1)}{\ell^2}\tilde{\kappa} - \frac{8(x_1^2-x_1^1)}{\ell^3}
\end{aligned} \tag{43}$$

where $\ell = \sqrt{(x_1^3 - x_1^1)^2 + (x_2^3 - x_2^1)^2}$. From the equations above we conclude that these derivatives are large when ℓ is small. Especially, this is the case when computing the neck curvature of two coalescing circles. Then the points $\mathbf{x}^1$ and $\mathbf{x}^3$ are the neighbouring points of the neck point $\mathbf{x}^2$.

When we take the nodal points fixed during the evolution, the nodes of the neck region are getting very close to each other, i.e. the approximate neck curvature has a large error (see also [13]). On the other hand, it seems reasonable that the collocation points have to lie close to each other in the neck region; since there we are expecting large variations of the velocity field of the boundary. These two conflicting aspects are brought together in an algorithm that takes care of the node distribution and which we describe first in the next subsection.

5.3 Node Distribution

In this subsection we present an algorithm for an optimal mesh generation which is based on equidistributing the curvature of the boundary. The aim of this algorithm is twofold. Firstly the number and place of the discretization points is optimized, which is important because the computational costs per time step are proportional to $(2N)^3$, where N is the number of points. Secondly this algorithm treats regions where a neck (or cusp) is occurring in a special way, see also the end of this subsection.

In this subsection we assume that the boundary of the fluid region can be described by a parametric equation with respect to the arc length s, i.e.

$$\mathbf{x}(s) \in \Gamma, \quad 0 \le s \le s_e \quad \text{and} \quad \mathbf{x}(0) = \mathbf{x}(s_e). \tag{44}$$

Only an equidistribution of the curvature is performed; an equidistribution of the velocity field of the boundary will not be necessary. In general, when the velocity and the curvature of the boundary are considered as functions of the arc length, we observed that the velocity function is a much "smoother" function than the curvature. Furthermore we observed that at places where the size of the velocity field is changing rapidly over a small part of the boundary, the curvature is also rapidly changing in size, i.e. the mesh is already finer there. When the velocity is large on a considerable part of the boundary, and the curvature is of moderate size everywhere, this part is moving as a whole but the shape as such is not deforming much, i.e. a finer mesh is not necessary.

First, we shall derive properties for the step-length between two successive nodes, which have to be fullfilled for all the mesh points that are generated. Let $\mathbf{x}^{i-1} = \mathbf{x}(s_{i-1})$ and $\mathbf{x}^{i} = \mathbf{x}(s_i)$ be two given successive nodal points and denote the distance between those points by $h_i = s_i - s_{i-1}$; the step-length. The next node $\mathbf{x}^{i+1}$ has to lie at a distance h_{i+1} from $\mathbf{x}_i$, such that the following conditions (45), (46) and (48) are satisfied.

We introduce two positive constants $h_{\min}$ and $h_{\max}$, which are given bounds for the step-length

$$h_{\min} \leq h_{i+1} \leq h_{\max}. \tag{45}$$

In effect, we are introducing a maximum resolution. Furthermore we want the collocation points to lie quasi-uniformly distributed on the boundary, i.e.

$$\frac{h_i}{k} \leq h_{i+1} \leq k h_i, \tag{46}$$

where k is a given parameter, larger than 1.

From (44) it follows that the curvature κ of the boundary can also be described as a function of the arc length s. We define the *curvature density*, say ε, of the curvature as follows

$$\int_\Gamma |\kappa(s)|\, ds \;=\; \mathrm{M}\,\varepsilon, \tag{47}$$

where M is a prescribed number, given by the user, and which is approximately equal to the total number of nodes that the algorithm will find eventually. The curvature of the boundary between two successive nodes integrated over the arc has to be smaller than this curvature density, i.e. the following equidistribution condition has to hold (approximately),

$$\int_{s_i}^{s_{i+1}} |\kappa(s)|\, ds \;=\; \varepsilon. \tag{48}$$

With h_ε we denote the step-length such that the equality from (48) holds, i.e. $s_{i+1} = s_i + h_\varepsilon$.

When the curvature is very large on a certain part of the boundary, i.e. in a neck region, it may happen that the proposed h_ε is smaller than the lower bound $h_{\min}$. However, we take as next step $h_{\min}$, although condition (48) is not satisfied then. A justification for this is given in the previous sections. There we have

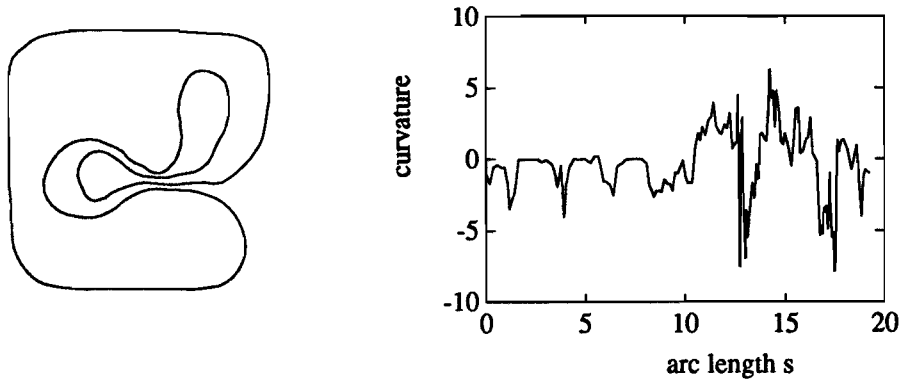

Figure 2: The curvature as function of the arc length s of the left figure. The derivative of this curvature with respect to the arc length is becoming large at some parts of the boundary, while the curvature is only moderately varying.

shown that it is not possible to approximate the correct neck curvature and that we have to proceed judiciously in choosing the "neck discretization": the neck point and its neighbouring points have to be chosen such that the neck curvature does not change (see also subsection 5.2).

From equations (45), (46) and (48), we see that the distance between $\mathbf{x}^i$ and the proposed next nodal point $\mathbf{x}^{i+1}$ is equal to

$$h_{i+1} \;=\; \max\Big(\, h_{\min},\, h_i/k,\, \min\big(\, h_{\max},\, kh_i,\, h_\epsilon \,\big)\Big). \tag{49}$$

However, this proposed h_{i+1} may be too large when it turns out that an appropriate step-length further on is not possible due to an increasing magnitude of the curvature; namely if at the next node, the step-length h_{i+2} is required to be equal to or larger than $\max(h_{\min}, h_{i+1}/k)$. Thus, we have to build in a mechanism that investigates whether the choice of node $\mathbf{x}^{i+1}$, i.e. step-length h_{i+1}, will not require the step-length for succeeding nodes to become larger than permitted!

At first sight, it seems obvious to choose a control mechanism that uses the derivative of the curvature with respect to the arc length s; however for a boundary with a rapidly changing though moderately valued curvature, the information of the derivative, derived numerically, is useless. See for example figure 2, taken from [3], in which the curvature with respect to the arc length of the above shape is plotted. Hence, we have developed the following simple algorithm for testing and correcting the step-length h_{i+1}.

We say that the step-length h_{i+1} is *a correct one*, when for all following smallest new step-lengths

$$\hat{s}_j \;:=\; s_i \,+\, \sum_{p=0}^{j} \frac{h_{i+1}}{k^p}, \qquad j = 0, ..., m, \tag{50}$$

where m is an integer such that $h_{i+1}/k^m \geq h_{\min}$ and $h_{i+1}/k^{m+1} < h_{\min}$, the

curvature equidistribution (48) holds,

$$\int_{\hat{s}_j}^{\hat{s}_{j+1}} |\kappa(s)|\, ds \;=\; \varepsilon, \qquad j = 0, ..., m-1. \tag{51}$$

When it follows that this h_{i+1} does not satisfy the above relation, this step-length is made somewhat smaller, i.e. $h_{i+1} = \max(h_{\min}, h_i/k, l * h_{i+1})$ where l is a given number, smaller than 1. Afterwards this new h_{i+1} is tested at the above described way. This procedure can be continued until the step-length is equal to $\max(h_{\min}, h_i/k)$.

This algorithm may look very time consuming; however, by choosing the bounds $h_{\max}/h_{\min} \approx 100$, say and the factor k is not too close to 1 this is not so dramatic. In our examples the CPU time for generating a complete mesh was a small percentage the costs per time step only.

Next, we discuss how a neck region is discretized. To dos this, we derive properties which have to be satisfied for the new discretized neck. We denote by $\mathbf{x}^n = \mathbf{x}(s_n)$ the neck point and by $\mathbf{x}^{n-1}$ and $\mathbf{x}^{n+1}$ the neighbouring nodes of the neck point, where $s_{n-1} < s_n < s_{n+1}$.

The first criterion that has to be satisfied is that the distance between the neighbouring nodes and the neck point is the *same*, and that the step-length is bounded as in (45), i.e.

$$h_{\min} \leq |s_n - s_{n-1}| = |s_{n+1} - s_n| \leq h_{\max}. \tag{52}$$

Furthermore, we have to avoid cancellation in the computation of the approximate neck curvature (see also [13]). This means that the distance between the neck point neighbours has to be larger than a certain bound $d_{\min}$, i.e.

$$\|\mathbf{x}^{n+1} - \mathbf{x}^{n-1}\| \geq d_{\min}, \tag{53}$$

where $d_{\min}$ is taken of the order $h_{\min}$ (we used $d_{\min} = 2h_{\min}$).

Another property is the equidistribution of the curvature, i.e. equation (48). In general, this condition is not fullfilled, when the neck curvature is large; however during the deformation of the neck region, the neck curvature is getting smaller and it may be possible that this condition can be satisfied.

From the above properties, we obtain a step-length, which is denoted by h_n, between the neck and the proposed new neighbouring neck points. The new approximate neck curvature, which is computed by fitting a quadratic interpolation polynomial through the neck node and its neighbours, is not the same as the old neck curvature. The size of this new neck curvature is unpredictable. However, we want to avoid the influence of this new neck curvature in the further computation. This is performed by *shifting* the neck point a bit such that the neck curvature is equal to the old curvature; more details can be found in the next subsection.

Using the ideas above, the collocation points are redistributed. If the boundary has neck regions, the node redistribution takes place starting from the discretized neck (where h_n is already known), to the middle of the boundary part

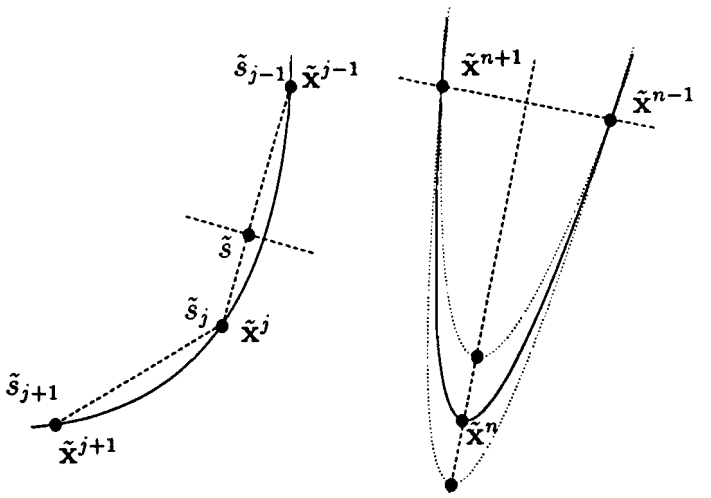

Figure 3: The first figure shows how the point $\tilde{\mathbf{x}}(\tilde{s})$ is found. The second figure is showing the direction in which the neck point is shifted, such that the neck curvature has a prescribed value.

between those necks. Afterwards, in the middle the nodes are somewhat shifted such that the mesh conditions (49) are satisfied. If the boundary does not have necks, one node of the old mesh is held fixed and the other nodes are generated relative to this fixed node. When the boundary is symmetric, a mesh generation is performed out on to symmetry part only, i.e. the nodes of the complete boundary are also chosen symmetrically.

5.4 Numerical Implementation of Node Distribution

In this subsection we comment on the numerical implementation of the algorithm which is given in subsection 5.1. First we introduce a discretized version of the arc length and show how a point $\mathbf{x}(s)$ is found. Furthermore, we discuss some properties about the neck discretization. Finally, we give the curvature equidistribution condition which is used in the numerical scheme.

In the numerical algorithm we are starting with an already discretized boundary, which will referred to as the *old* nodes $\tilde{\mathbf{x}}^i$ $(1 \leq i \leq \mathrm{N})$. For practical application of applying the ideas of the previous subsection, we have to define a discretized version of the arc length, say $\tilde{s}$, i.e. how a point $\tilde{\mathbf{x}}(\tilde{s})$ has to be found, and what is meant by the curvature $\tilde{\kappa}(\tilde{s})$.

In the numerical algorithm we use as a discretization of the arc length the straight-line distance between two successive old nodes, i.e.

$$\tilde{s}_i = \tilde{s}_{i-1} + \|\tilde{\mathbf{x}}^i - \tilde{\mathbf{x}}^{i-1}\| \quad (2 \leq i \leq \mathrm{N}+1), \tag{54}$$

where $\tilde{s}_1 = 0$ and $\tilde{\mathbf{x}}^{\mathrm{N}+1} = \tilde{\mathbf{x}}^1$. A nodal point at a certain arc length, say $\tilde{s}$, is found by fitting a quadratic polynomial through tree successive old nodes, say

$\tilde{\mathbf{x}}^{j-1}$, $\tilde{\mathbf{x}}^{j}$ and $\tilde{\mathbf{x}}^{j+1}$, where j is taken such that

$$|\tilde{s}_j - \tilde{s}| \;\leq\; \min\Big(|\tilde{s}_{j-1} - \tilde{s}|,\, |\tilde{s}_{j+1} - \tilde{s}|\Big). \tag{55}$$

Assuming that $\tilde{s} < \tilde{s}_j$, the node $\tilde{\mathbf{x}}(\tilde{s})$ is at the intersection of this quadratic polynomial with the straight line in the direction normal to the straight line through the old points '$j-1$' and 'j', and through the point on this straight line that has a distance $\tilde{s}_j - \tilde{s}$ with the node $\tilde{\mathbf{x}}^j$ (see figure 3).

However, the proposed new neighbouring neck points are computed using a straight line representation through the two successive old nodes which are lying between the proposed arc length ($\tilde{s} = \tilde{s}_n \pm h_n$). A linear interpolation is carried out instead of a quadratic interpolation; this is to avoid interpolation errors which occur when the neck curvature is large and the old nodes are not distributed nice in the neck region.

We also require that the new approximate neck curvature is equal to the old neck curvature. To perform this, the neck point is shifted a bit over the straight line through the old neck point, in the direction normal to the straight line through the new neighbouring nodes; or, when the new nodes are lying further apart than the old neighbours, through these old nodes (see also figure 3). The neck node may be shifted over a maximum a distance $d_{\max}$, i.e.

$$\|\tilde{\mathbf{x}}^n - \mathbf{x}^n\| \;\leq\; d_{\max}, \tag{56}$$

where $d_{\max}$ is also of the order $h_{\min}$ (we used $d_{\max} = 0.25 h_{\min}$). If it is not possible to find a new neck point on this line, the neck point is shifted over a distance $d_{\max}$ on this line, such that the new neck curvature is as close as possible to the old curvature.

When starting a computation, the curvature of the neck points of the initial boundary are unknown. These initial neck curvatures may be user specified, or they are computed from the initial nodes.

The approximate curvature $\tilde{\kappa}_i$ of the old nodes is found in the usual way, see subsection 5.2. The curvature at a certain value of the arc length, i.e. $\tilde{\kappa}(\tilde{s})$, is derived in the same way as a boundary point was found; however, now through linear interpolation. In our algorithm we derive an approximation of h_ε using the linear discrete form of (48), which is given by

$$h_\varepsilon\Big(|\tilde{\kappa}(\tilde{s}_i + h_\varepsilon)| + |\tilde{\kappa}(\tilde{s}_i)|\Big) \;=\; 2\varepsilon. \tag{57}$$

This equation is solved using a bisection method.

6 Numerical Results and Discussion

In this section we shall demonstrate the usefulness of the node redistribution algorithm, as described in section 5.3; we show a number of results for some simply connected surfaces. All problems are solved using quadratic boundary elements. Since, as we said in the introduction, the driving force for sintering arises from the

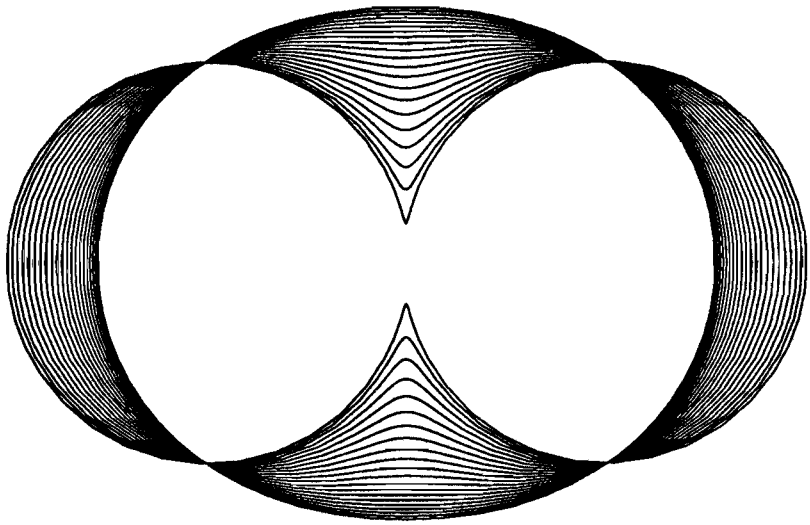

Figure 4: The coalescence of two equal circles in time. The boundary curves refer to values of time $t = 0.0(0.1)2.0$.

excess of free surface energy, a 2-dimensional viscous incompressible fluid region Ω transforms itselfs into a circle, and the total surface of the region has to remain constant, when the time is going to infinity.

The first example is the coalescence of two equal circles, see also figure 4. We shall compare the derived numerical results with the analytical solution of section 3. For the initial radius R is taken $\frac{1}{2}\sqrt{2}$; than the final shape of the coalescence is a circle with radius 1. The contact radius r is set equal to 0.14. Using this and equation (21), it follows that the exact neck curvature is approximately equal to 707. The centre of mass is taken as the reference point, which is chosen to be the origin. The initial nodes of the shape are derived from the exact solution. Only nodes from the first quadrant are needed because of the double symmetry of the body. This symmetry is preserved during the calculation. For the node distribution algorithm we used as bounds for the step length, $h_{\min} = 0.005$ and $h_{\max} = 0.15$; for the uniformly distribution factor k taken 1.5 and we have taken the number M equal to 15 for the shape of the first quadrant.

In figure 4 we have plotted the transformation of the fluid region in time with initial neck curvature equal to 700. The curves are given between the (dimensionless) time $t = 0.0$ and $t = 2.0$ with time intervals of 0.1. In figure 5 we compare the neck curvature obtained by the numerical simulation (solid line) with the analytical curvature of the neck (dotted line). It can be observed that the numerical neck curvature differs quite a bit from the exact curvature in the early stage of the coalescence; but when time is increasing, both curvatures are getting very close

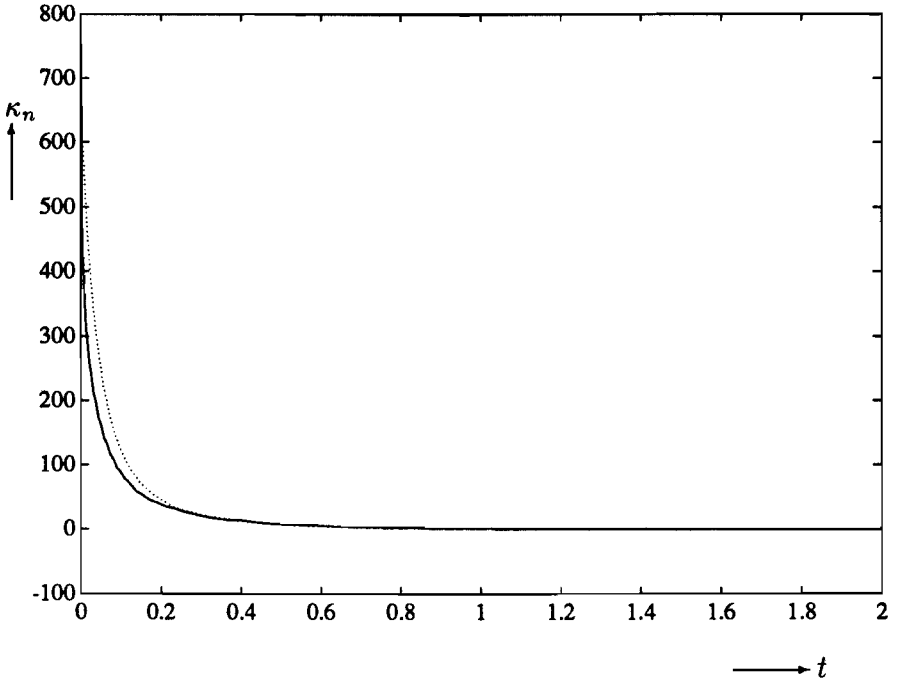

Figure 5: The neck curvature obtained by numerical simulation (solid line), is compared with the analytical curvature of the neck (dotted line) over a large period of time.

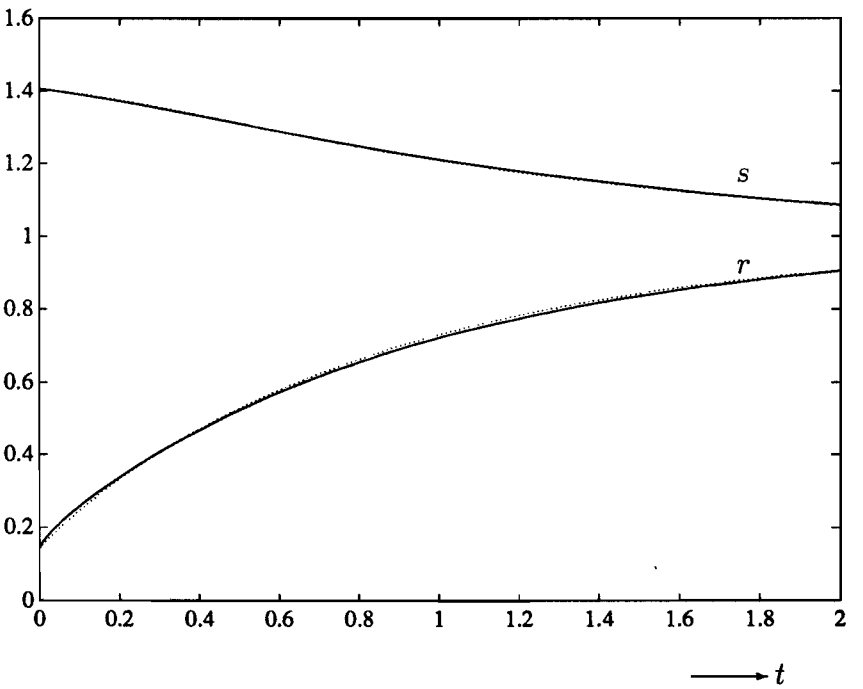

Figure 6: The contact radius r and the shrinkage s, both obtained by numerical simulations (solid lines), are compared with the analytical solutions (dotted lines) over a large period of time.

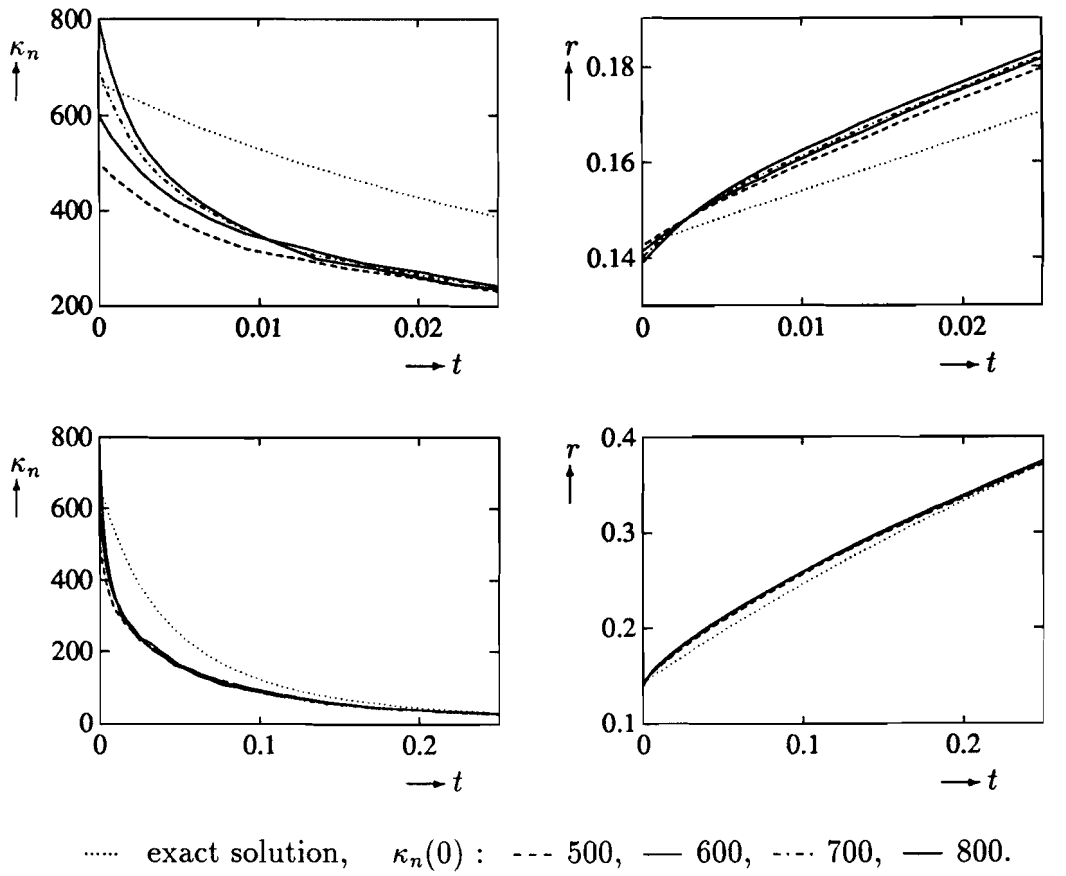

Figure 7: The neck curvature obtained by the numerical simulation, with initial curvature set equal to 500, 600, 700 and 800 respectively, are compared with the analytical curvature of the neck (dotted line). The derived numerical contact radius r is also compared with the analytical solution.

to each other. In figure 6 we have plotted the contact radius r and the shrinkage s obtained both by the numerical and analytical solution. When we compare the numerical contact radius (solid line) with the analytical contact radius (dotted line), we see that these lines are almost the same, even in the initial stage.

When we zoom in to this initial stage to get a better look of the development of the obtained neck curvature and contact radius, we obtain the pictures of figure 7; they also demonstrate the influence of the initial neck curvature on the development of the neck curvature and contact radius. We have set this initial neck curvature equal to 500, 600, 700 and 800 respectively. The derived neck curvatures and contact radii are compared to the analytical solutions (dotted lines). It can be observed that the obtained numerical curvatures are getting close to each other after a small period of time; but they significantly differ from the analytical solution. After a small period of time, the lines of the numerically derived contact radii run all parallel to each other. This can be interpreted as a small shift in *time*. When we compare these numerical contact radii with the exact solution, we see that those lines run also roughly parallel to each other, i.e. the time is also a little moved on. This is due to spatial and time discretization errors.

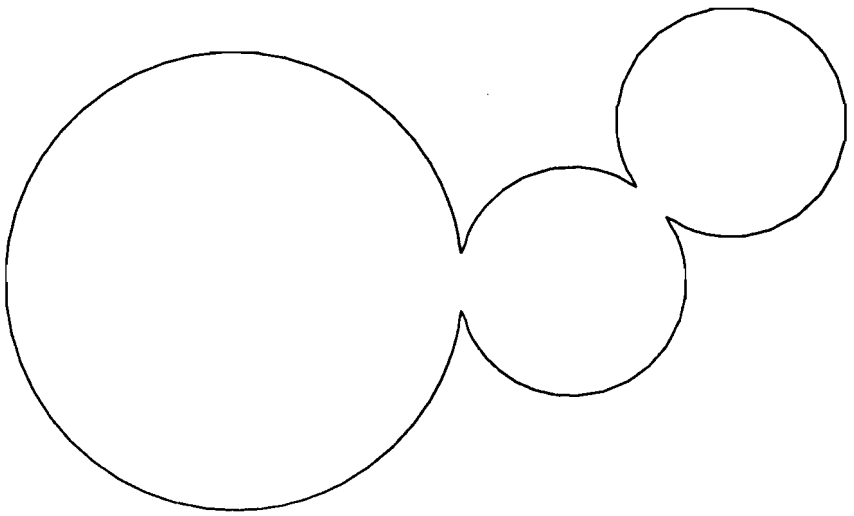

Figure 8: The initial fluid region which are three coalescing circles.

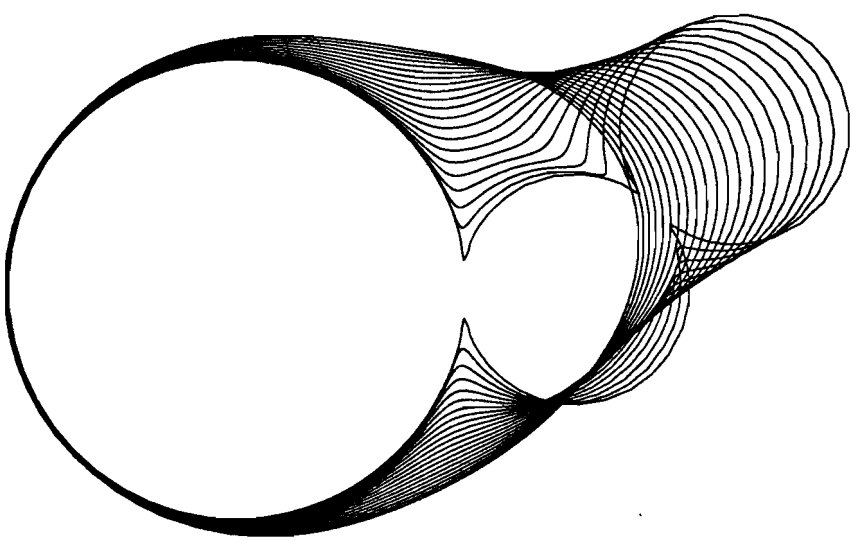

Figure 9: The coalescence of this three circles in time. The boundary curves refer to values of time $t = 0.0(0.1)2.0$.

Note that the development of the shape is most important; the (dimensionless) time is not an important parameter because in reality, sintering can last a few minutes up to a few days.

The above results are illustrating the correctness of the conclusions which we derived from the perturbation analysis as is carried out in section 4. Thus if the approximate neck curvature is of the order of the exact neck curvature, then this will hardly change the development of the contact radius between both circles.

Another example to demonstrate the node redistribution algorithm is the shape which is plotted in figure 8. The initial radius of the largest circle is taken equal to 1 and the radii of both small circles are set equal to 0.5. The centre of the largest circle is the origin and again, this point is chosen to be the reference point. The angle between the straight lines through the centres of those circles is equal to 45 degrees. The contact radius of both small circles was initially equal to 0.095 and the other was set equal to 0.13. Furthermore, we used the analytical solution for the coalescence of two equal circles (15) to approximate the initial neck regions. The boundary of the touching region between the large and small circle is approximated at the following way: for the neck region on the side of the largest circle we used the analytical solution with $R = 1$; for the other side from the neck point, we used the analytical solution with $R = 0.5$. The transformation of these circles in time is shown in figure 9.

At last, we consider the geometry of three equal circles, which are making an angle with each other, i.e. a problem with one axis of symmetry, see also the solid lined shape of figure 10. This three particle model is commonly used in sintering literature to study the effect of packing irregularities. The origin is set in the centre of the circle in the middle, which is also used as reference point. The radii of those circles are taken equal to 0.5, and for the angle between the centres of the circles we took 70 degrees. Again, the neck region is approximated using the analytical solution. However, here we used different neck regions, i.e. neck curvatures, on both sides of the contact line between two touching circles. We derived the neck region with smallest curvature, i.e. the outer neck, using a contact radius of 0.2 and on the other side (inner neck) we took the contact radius equal to 0.075. From equation (21), this choice of contact radii is giving a neck curvature approximately equal to 110 an 2330 for the outer and inner neck respectively.

The dotted shape of figure 10 is obtained at time $t = 0.1$. When comparing this shape with the initial configuration, it can be seen that the circles are rotated. This effect is also observed in reality when three glasses spheres are sintered, see also Petzow and Exner [9] or Sōmiya and Moriyoshi [11], pp. 649. From this we conclude that the neck growth, which is a local process, can influence the global shape evolution. Thus a numerical approach which consists of decomposing the boundary in neck regions and smooth parts and computing these more or less separately, would not be able to simulate this effect, i.e. such a method is incorrect.

In figure 11 we show the obtained shape evolution between $t = 0.0$ and $t = 2.0$ with time intervals of 0.1. We see that two necks on the inner side grow together

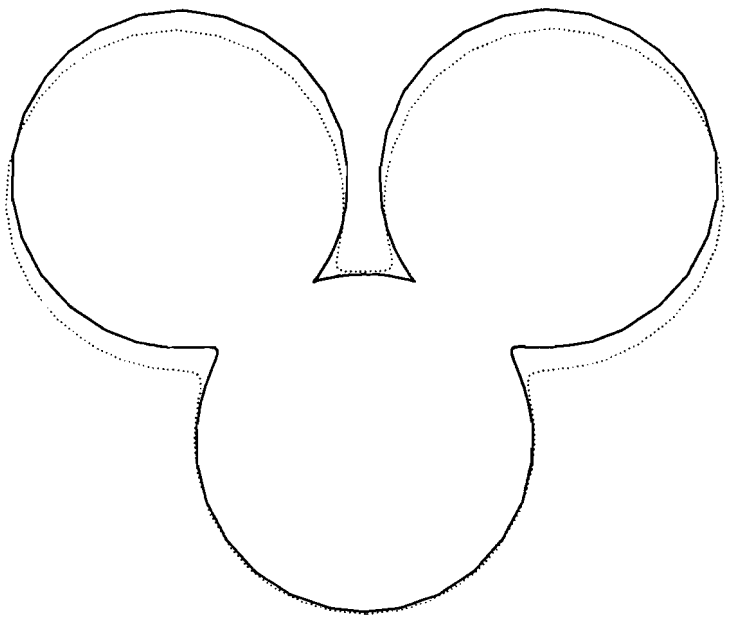

Figure 10: The initial fluid region (solid line) which consist of three equal coalescing circles with an angle between the centres of 70 degrees. The dotted lined shape is the fluid at $t = 0.1$, which is showing the angle change during the evolution.

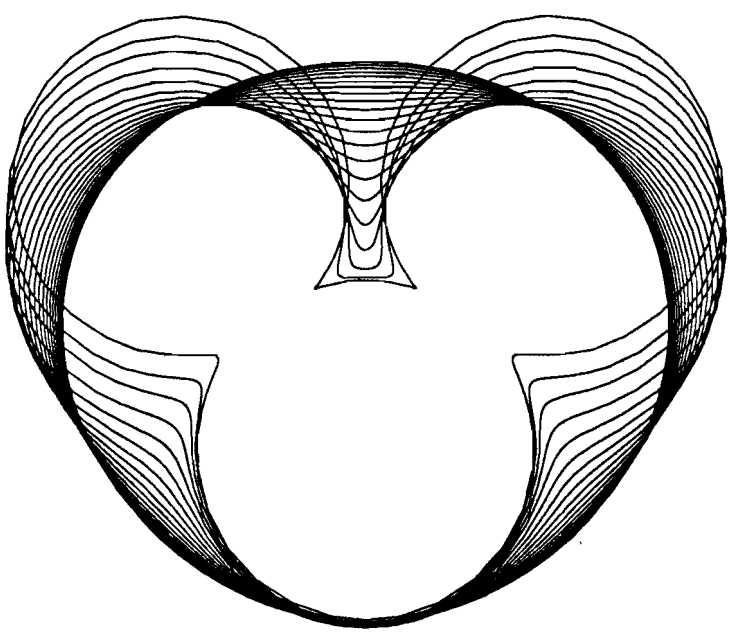

Figure 11: The coalescence of this three equal circles in time. The boundary curves refer to values of time $t = 0.0(0.1)2.0$.

and this is showing that our algorithm is able to simulate this effect also.

In future, we plan to investigate multiply connected regions, i.e. viscous fluid regions with gas bubbles.

ACKNOWLEDGMENT

This research was supported by the Technology Foundation (STW).

References

[1] DRITSCHEL D.G., Contour Surgery: A Topological Reconnection Scheme for Extended Integrations Using Contour Dynamics, *J. Comput. Phys.* **77**, 240-266 (1988).

[2] GRADSHTEYN I.S., RYZHIK I.M., Table of Integrals, Series, and Products, transl. A. Jeffrey, Corrected and Enlarged Edition, Academic Press, New York, (1980).

[3] HOPPER R.W., Plane Stokes flow driven by capillarity on a free surface, *J. Fluid Mech.* **213**, 349-375, (1990).

[4] HOPPER R.W., Plane Stokes Flow driven by capillarity on a free surface, 2: Further Developments, *J. Fluid Mech.* **230**, 355-364, (1991).

[5] HSIAO G.C., KOPP P., WENDLAND W.L., Some applications of a Galerkin-collocation method for boundary integral equations of the first kind, *Math. Methods in the Appl. Sciences* **6**, 280-325, (1984).

[6] JAGOTA A. AND DAWSON P.R., Micromechanical Modeling of Powder Compacts-I. Unit Problems for Sintering and Traction-Induced Deformation, *Acta. Metall.* **36**, 2551-2561, (1988).

[7] KUIKEN H.K., Viscous sintering: the surface-tension-driven flow of a liquid form under the influence of curvature gradients at its surface, *J. Fluid Mech.*, **214**, 503-515, (1990).

[8] LADYZHENSKAYA O.A., The Mathematical Theory of Viscous Incompressible Flow, Gordon and Beach, New York, (1963).

[9] PETZOW G., EXNER H.E., Particle Rearrangement in Solid State Sintering, *Zeitschrift für Metallkunde*, **67**, 611-618, (1976).

[10] ROSS J.W., MILLER W.A. AND WEATHERLY G.C., Dynamic Computer Simulation of Viscous Flow Sintering Kinetics *J. Appl. Phys.* **52**, 3884-3888, (1981).

[11] SŌMIYA S., MORIYOSHI Y. (Eds.), Sintering Key Papers, Elsevier Applied Science, London, (1990).

[12] VORST G.A.L. VAN DE, MATTHEIJ R.M.M., Implementing the Boundary Element Method for 2-D Viscous Sintering, in *Proc. Conf. on Computational Modelling of Free and Moving Boundary Problems, Vol.1 Fluid Flow*, edited by L.C. Wrobel and C.A. Brebbia, Computational Mechanics Publications, Southampton, U.K, 341-355, (1991).

[13] VORST G.A.L. VAN DE, MATTHEIJ R.M.M., KUIKEN H.K., A boundary element solution for 2-dimensional viscous sintering, To appear in *J. Comput. Phys.*, (1992).